Received: 22 July 2024 | Revised: 17 August 2024 | Accepted: 5 September 2024

DOI: 10.1002/joa3.13148

Journal of Arrhythmia Open Access WILEY

ORIGINAL ARTICLE

Predictability of indicators in local activation time mapping of ablation success for premature ventricular contractions

Takahiko Nagase MD, PhD | Takafumi Kikuchi MD | Shun Akai MD | Masafumi Himeno MD | Ryo Ooyama MD | Yoshinori Yoshida MD | Chiyo Yoshino MD | Takafumi Nishida MD | Takahisa Tanaka MD | Mitsunori Ishino MD, PhD | Ryuichi Kato MD, PhD | Masao Kuwada MD

Department of Cardiology, Higashiyamato Hospital, Tokyo, Japan

Correspondence
Takahiko Nagase, Department of Cardiology, Higashiyamato Hospital, 1-13-12 Nangai, Higashiyamato-shi, Tokyo 207-0014, Japan.
Email: takahiko.nagase@yamatokai.or.jp

Abstract

Introduction: Differences in predictability of ablation success for premature ventricular contractions (PVCs) between earliest isochronal map area (EIA), local activation time (LAT) differences on unipolar and bipolar electrograms ($\Delta LAT_{Bi\text{-}Uni}$), LAT prematurity on bipolar electrograms (LAT_{Bi}), and unipolar morphology of QS or Q pattern remain unclear. We verified multiple statistical predictabilities of those indicators of ablation success on mapped cardiac surface.

Methods: Thirty-five patients with multiple PVCs underwent catheter ablation after LAT mapping using multipolar mapping catheters with unipolar-based annotation. Patients were divided into success and failure groups based on ablation success on mapped cardiac surfaces. Discrimination ability, reclassification table, calibration plots, and decision curve analysis of 10 ms EIA (EIA_{10ms}), $\Delta LAT_{Bi\text{-}Uni}$, and LAT_{Bi} were validated. Unipolar morphology was compared between success and failure groups.

Results: Right ventricular outflow tract, aortic cusp, and left ventricle were mapped in 17, 10, and 8 patients, respectively. In 14/35 (40%) patients, successful ablation was performed on mapped cardiac surfaces. Area under the curve of receiver-operating characteristic curve of EIA_{10ms}, $\Delta LAT_{Bi\text{-}Uni}$, and LAT_{Bi} were 0.874, 0.801, and 0.650, respectively (EIA_{10ms} vs. LAT_{Bi}, $p = .014$; $\Delta LAT_{Bi\text{-}Uni}$ vs. LAT_{Bi}, $p = .278$; EIA_{10ms} vs. $\Delta LAT_{Bi\text{-}Uni}$, $p = .464$). EIA_{10ms} and $\Delta LAT_{Bi\text{-}Uni}$ demonstrated better predictability, calibration, and clinical utility on reclassification table, calibration plots, and decision curve analysis than LAT_{Bi}. Unipolar morphology of QS or Q pattern did not correlate with ablation success ($p = .518$).

Conclusion: EIA_{10ms} and $\Delta LAT_{Bi\text{-}Uni}$ more accurately predict ablation success for PVCs on mapped cardiac surfaces than LAT_{Bi} and unipolar morphology.

KEYWORDS
bipolar prematurity, earliest isochronal map area, local activation time difference, premature ventricular contraction, unipolar prematurity

1 | INTRODUCTION

Catheter ablation is established as an effective therapeutic choice for symptomatic multiple premature ventricular contractions (PVCs) or PVCs with left ventricular dysfunction.[1,2] Earliest isochronal map area (EIA), local activation time (LAT) differences on unipolar and bipolar electrograms ($\Delta LAT_{Bi\text{-}Uni}$), LAT prematurity on bipolar electrograms (LAT_{Bi}), and unipolar morphology of QS or Q pattern have been reported as indicators of ablation success.[3–8] Recently, high-density mapping using multipolar mapping catheters has been shown to be effective for identifying origin of PVCs by accurate LAT mapping.[9] Hower, those indicators have not been compared as prediction models, using multiple statistical analyses including discrimination, reclassification, calibration or clinical utility in the era of high-density mapping.

Therefore, we verified the predictability of ablation success of EIA, $\Delta LAT_{Bi\text{-}Uni}$ and LAT_{Bi} obtained from high-density LAT maps as prediction models along with correlation with ablation success and unipolar morphology of QS or Q pattern.

2 | METHODS

2.1 | Study subjects and design

From September 2018 to December 2023, 35 consecutive patients, in whom LAT maps of PVCs were made by multipolar mapping catheters in ablation of symptomatic multiple PVCs with CARTO3 system (Biosense Webster, Diamond Bar, CA), were enrolled. Cardiac surface estimated as the origin of PVCs based on the 12-lead electrocardiogram was mapped depending on operators' discretion or previous reports.[10–14] No patient underwent ablation based on the pace-mapping. In this study, LAT maps of right ventricular outflow tract, left ventricle, and coronary cusps were initially created and evaluated. Regarding the mapped cardiac surfaces of left ventricle, left ventricular outflow tract, mitral valve annulus, and left ventricular posteroseptum were included.

The patients, in whom PVCs were abolished by ablation only on initial mapped cardiac surfaces, were defined as success group. Those, in whom ablation on the contralateral cardiac surfaces (e.g., left ventricular outflow tract or coronary cusps in the case of initial ablation surface of right ventricular outflow tract) was required or PVCs did not ultimately disappear, were classified into failure group. EIA, $\Delta LAT_{Bi\text{-}Uni}$, LAT_{Bi}, and unipolar morphology of QS or Q pattern were compared offline after procedures between success and failure groups.

We assessed the following aspects of predictability of the indicators (1) discrimination ability, (2) reclassification, (3) calibration ability, and (4) clinical usefulness of 10 ms EIA (EIA10ms), ΔLATBi-Uni, and LATBi, and (5) differences on the rate of unipolar morphology of QS or Q pattern between success and failure groups. Regarding discrimination ability, area under the curve (AUC) by receiver-operating characteristic curve was compared between the indicators and optimal cutoff value of each indicator was calculated. Net reclassification improvement (NRI) and integrated discrimination improvement (IDI) were evaluated on the reclassification tables. Calibration ability and clinical usefulness were validated on calibration plots and decision curve analysis, respectively. The study was approved by the local institutional review board (local ethics committee number: 2023–026) and was conducted according to the principles of the Declaration of Helsinki. All patients provided informed consent.

2.2 | LAT mapping and ablation of PVCs

LAT maps of PVCs were created without isoproterenol infusion using DECANAV catheters (Biosense Webster) with 1 mm width electrodes and an interelectrode spacing of 2–8–2 mm for right ventricular outflow tract and 5-spline PentaRay catheters (Biosense Webster) with 1 mm width electrodes and an interelectrode spacing of 2–6–2 mm or 8-spline OctaRay catheters (Biosense Webster) with 0.5 mm width electrodes and an interelectrode spacing of 2–2–2-2-2 mm for left ventricles or coronary cusps. LAT maps were created with Pattern Matching Filter (Biosense Webster) using the algorithm annotating on the bipolar distal electrodes the timing of unipolar steepest dV/dT that coincides with a bipolar potential (WaveFront, Biosense Webster). Annotation reference was set based on 12-lead electrocardiogram using the equipped algorithm (advanced reference annotation, Biosense Webster). Surface and intracardiac electrocardiograms were recorded using an EP-system (RMC-5000, Nihon Kohden, Tokyo, Japan).

After LAT mappings, earliest sites on bipolar electrograms were validated near earliest color areas using saline-irrigated contact force sensing catheters (Thermocool SmartTouch Surround Flow, Biosense Webster). Ablation was initially performed on the mapped cardiac surfaces. Ablation sites were targeted at the bipolar earliest site with confirmation of unipolar morphology on the EP-system. LAT maps were not converted to isochronal maps during the procedures. Ablation was performed with 25–40 W with a maximum temperature of 40°C within impedance drops of ≤15 ohm for 60–90 s. Ablation success site was defined as elimination of PVCs within 30 s. If ablation at the bipolar earliest site did not abolish PVCs, the adjacent earliest activation sites were cauterized. If 10–15 applications could not suppress PVCs, the bipolar earliest site of the adjacent contralateral cardiac surfaces were similarly ablated. No epicardial ablation except for that via intracoronary sinus was not performed. The procedural endpoint was defined as disappearance of PVCs after 30 min waiting time and administration of isoproterenol (1–3 μg/min).

2.3 | Measurements of indicators

EIA_{10ms} was measured offline after LAT maps of PVCs were converted to isochronal maps with 10 ms steps. Obvious incorrect

annotations were deleted. The minimum density of points required to conclude that the electroanatomic map of a given chamber was acceptable was defined as a fill threshold of 15 mm as previously described.[3,4]

$\measuredangle LAT_{Bi\text{-}Uni}$, LAT_{Bi}, and unipolar morphology of QS or Q pattern were recorded offline at a sweep speed of 400 mm/s on CARTO3 system. The high- and low-pass filters were 16 and 500 Hz, respectively, for bipolar electrograms and 2 and 240 Hz, respectively, for unipolar electrograms. Surface electrograms were filtered with a low-pass of 0.5 Hz and a high-pass of 120 Hz.

$\measuredangle LAT_{Bi\text{-}Uni}$ was recorded at the point of earliest steepest dV/dT on unipole automatically annotated by WaveFront (Biosense Webster) and was defined as the absolute value of LAT difference between earliest LAT on bipole and timing of steepest dV/dT on unipole of the distal electrode of the same bipole. Because earliest sites by WaveFront (Biosense Webster) and manual bipolar annotation show good correlation,[15] LAT_{Bi} was measured at or near the earliest sites identified by WaveFront (Biosense Webster) within EIA_{10ms} and was defined as LAT difference between earliest bipolar deflection and QRS onset. Unipolar morphology of QS or Q pattern was evaluated at the point of the earliest sites identified by WaveFront (Biosense Webster). All the indicators were assessed similarly both in both success and failure groups. An example of measurements is shown in Figure 1A,B. The correlation between EIA_{10ms}, $\measuredangle LAT_{Bi\text{-}Uni}$, and LAT_{Bi} were also calculated.

2.4 | Follow-up

Antiarrhythmic drugs were discontinued after procedures. Patients attended outpatient visits 1 month after procedures and every 3 months thereafter. Twelve-lead electrocardiograms at each visit and 24 h Holter monitoring every 6 months after procedures were evaluated for recurrence of PVCs.

2.5 | Statistical analysis

Continuous variables with a normal distribution and nonparametric variables are presented as means ± standard deviation and the median and interquartile range, respectively. To compare continuous variables with normal distribution and nonparametric variables, we used Student *t* test and Mann–Whitney U test, respectively. Categorical variables are expressed as number and percentage and were compared using χ^2 test between success and failure groups.

Regarding sample size estimation, there is no generally accepted approach for the estimation of the sample size for derivation of risk prediction models.[16] However, previous studies validating EIA or $\measuredangle LAT_{Bi\text{-}Uni}$ for ablation success analyzed 15–70 patients.[3–6] Also, Herczku et al.[3] reported that the median differences and interquartile range of EIA_{10ms} on right ventricular outflow tract differentiating

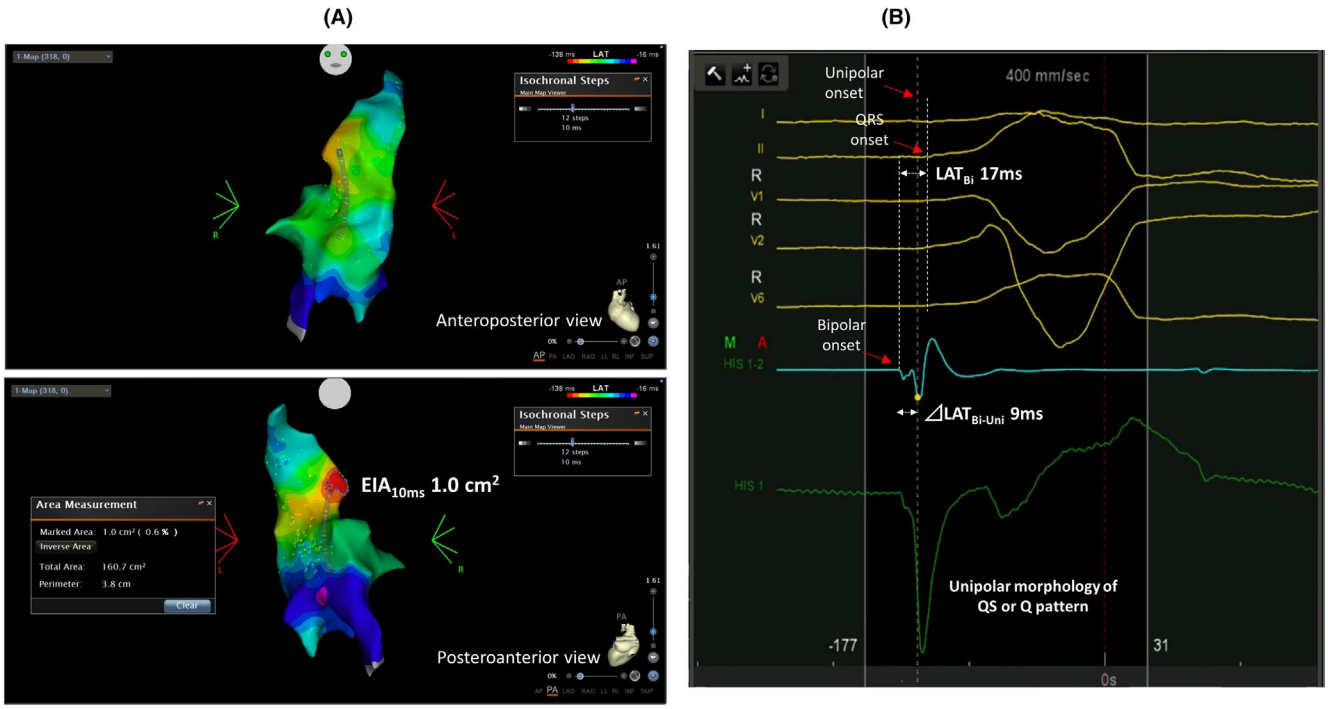

FIGURE 1 Measurements of indicators of ablation success. (A) An example of successful ablation on posterolateral wall of right ventricular outflow tract (upper, anteroposterior view; lower, posteroanterior view). (B) Intracardiac electrocardiograms at the point of earliest steepest dV/dT on unipole. ⊿LATBi-Uni, local activation time (LAT) differences on unipolar and bipolar electrograms; EIA10ms, 10 ms earliest isochronal map area; LATBi, LAT prematurity on bipolar electrograms.

PVC origins of right or left ventricular outflow tracts was 2 cm^2 and 1 cm^2, respectively. Based on those values, the required sample size was calculated with detection difference of 2 cm^2, standard deviation of 1 cm^2, alpha error of 0.05, and power of 0.8, and was estimated as at least 34 patients.

Logistic regression models were prepared for prediction of ablation success on the mapped cardiac surfaces and were assessed by goodness-of-fit test using χ^2 test with $p = .948$, which indicated overall performance of predictabilities of evaluated indicators. Discrimination ability, cutoff values and reclassification of indicators of ablation success were validated as described above. Calibration ability was assessed by evaluating how much the slope of the calibration line (plotting the predicted probabilities vs. the observed probabilities) deviates from the ideal of 1.0 and intercept of 0.0. We used a bootstrapping procedure with 1000 samples drawn with replacement from the original sample to assess the internal validation of the model. Decision curve analysis to indicate the net benefit and clinical utility of the indicators were performed as previously described.[17,18] The correlation between EIA_{10ms}, $\measuredangle LAT_{Bi\text{-}Uni}$, and LAT_{Bi} were calculated with Spearman's rank-correlation coefficient. A p value of <.05 was considered statistically significant. All data were calculated using JMP version 16.2.0 (SAS Institute, Inc, Cary, NC) and R (version 4.2.0, The R Foundation for Statistical Computing).

3 | RESULTS

3.1 | Patient characteristics

In 40% of all patients, coronary artery disease or other structural heart disease are complicated. The ratio of those underlying diseases, left ventricular ejection fraction and brain natriuretic peptide did not differ between success and failure groups. Mean burden of PVCs on Holter electrocardiograms was 23% without any statistical differences between groups. Repeat procedures were involved in one patient in success group and in one patient in failure group.

Electrocardiographic features of PVCs were classified into three types; right bundle branch block plus inferior axis, left bundle branch block plus inferior axis, and right bundle branch block plus superior axis. The features of PVCs including R/S amplitude ratio, R/S duration ratio, and V2 S/V3 R amplitude ratio were similar between success and failure groups. Details are summarized in Table 1.

3.2 | Procedural and mapping data and clinical outcome

PVCs were successfully ablated in 32/35 (91%) patients. Successful ablation sites were within EIA_{10ms} in all patients in success group. Ablation of contralateral cardiac surfaces was performed in all patients in failure group. Procedure and fluoroscopy time were longer in failure group than success group (both, $p < .001$). All patients were ablated through endocardial access. Ablation in coronary sinus was performed in only two patients in failure group.

Initial mapped cardiac surfaces were right ventricular outflow tract, left ventricle, and coronary cusps in 49%, 23%, and 29% of all patients, respectively, and did not differ between success and failure groups. Mapping points and fill thresholds of isochronal maps on the initial mapped cardiac surfaces were not different between the groups. EIA_{10ms} and $\measuredangle LAT_{Bi\text{-}Uni}$ were smaller in success group than in failure group (both, $p < .01$), while LAT_{Bi} was similar between groups. Details are summarized in Table 2.

During a mean follow-up of 14 ± 8 months, PVCs were suppressed at PVC burden of <5% on 24-h Holter monitoring in all patients with ablation success at the end of procedures.

3.3 | Discrimination ability, reclassification table, and correlation of unipolar morphology with ablation success

AUCs of EIA_{10ms}, $\measuredangle LAT_{Bi\text{-}Uni}$, and LAT_{Bi}, were 0.87, 0.80, and 0.62, respectively. Comparison of AUCs between each two indicators revealed the superiority of EIA_{10ms} on discrimination ability than LAT_{Bi} ($p = .014$; others, p = NS) (Figure 2A and Table 3). Receiver-operating characteristic curve analysis demonstrated that optimal cutoff values for ablation success of EIA_{10ms}, $\measuredangle LAT_{Bi\text{-}Uni}$, and LAT_{Bi} were 1.2 cm^2, 9 ms, and 7 ms, respectively (Table 3). Regarding each cutoff values of EIA_{10ms} in different cardiac chambers, optimal cutoff values were 1.2 cm^2, 1.5 cm^2, and 0.1 cm^2 in right ventricular outflow tract, left ventricle, and coronary cusps, respectively (right ventricular outflow tract, AUC 0.85, sensitivity 75.0%, specificity 88.9%; left ventricle, AUC 0.94, sensitivity 100.0%, specificity 75.0%; coronary cusps, AUC 0.69, sensitivity 50.0%, specificity 100.0%). However, the number of patients per cardiac chamber was small (especially for coronary cusps), and those analyses were only reference values.

In reclassification tables, EIA_{10ms} demonstrated better predictability for ablation success than $\measuredangle LAT_{Bi\text{-}Uni}$ and LAT_{Bi} for NRI and/or IDI (all, $p < .05$) (Table 3). $\measuredangle LAT_{Bi\text{-}Uni}$ showed better predictability on NRI than LAT_{Bi} ($p = .020$). Unipolar morphology did not correlate with ablation success ($p = .518$) (Figure 2B). An example of failure group is shown in Figure 3.

3.4 | Calibration plots and decision curve analysis

Calibration plot of each indicator is shown in Figure 4A–C. Along with better calibration slope and intercept, EIA_{10ms} and $\measuredangle LAT_{Bi\text{-}Uni}$ visually represented better correlation with the predicted probabilities vs. the observed probabilities compared with LAT_{Bi}.

Decision curve analysis of the indicators including unipolar morphology revealed that net benefit was higher in order of small EIA_{10ms}, small $\measuredangle LAT_{Bi\text{-}Uni}$, LAT_{Bi}, and unipolar morphology of QS or Q pattern

TABLE 1 Baseline characteristics.

	All patients $n = 35$	Success $n = 14$	Failure $n = 21$	p value*
Age (years)	61 ± 17	54 ± 18	65 ± 15	.087
Male	19 (54)	6 (43)	13 (62)	.268
Hypertension	16 (46)	5 (36)	11 (52)	.491
Diabetes mellitus	7 (20)	1 (7)	6 (29)	.203
Coronary artery disease	5 (14)	3 (21)	2 (10)	.369
Structural heart disease[a]	9 (26)	4 (29)	5 (24)	1.000
Atrial fibrillation	2 (6)	1 (7)	1 (5)	1.000
Left ventricular ejection fraction (%)	60 ± 8	62 ± 8	58 ± 6	.116
BNP (pg/ml)	97 (29–215)	90 (53–196)	25 (114–223)	.753
Previous ablation	2 (6)	1 (7)	1 (5)	1.000
PVC burden (%)	23.2 ± 10.7	22.2 ± 10.2	24.0 ± 11.2	.627
Electrogram characteristics of PVC				
RBBB pattern + inferior axis	14 (40)	4 (29)	10 (48)	.311
RBBB pattern + superior axis	2 (6)	1 (7)	1 (5)	1.000
LBBB pattern + inferior axis	19 (54)	9 (64)	10 (48)	.332
R/S amplitude ratio in V1	0.29 (0.13–1.67)	0.07 (0.16–2.25)	0.14 (0.67–3.25)	.162
R/S amplitude ratio in V2	0.15 (0.36–3.25)	0.30 (0.15–2.2)	0.71 (0.19–4.34)	.409
R/S duration ratio in V1	0.60 (0.50–2.00)	0.5 (0.38–1.25)	1 (0.50–2.00)	.057
R/S duration ratio in V2	1.00 (0.50–2.00)	0.50 (0.38–2.13)	1.00 (0.50–2.75)	.248
V2 S/V3 R amplitude ratio	2.00 (0.25–4.00)	1.8 (0.18–4.00)	3.15 (0.33–4.68)	.567

Note: Values are presented as mean ± standard deviation, n (%), or median (interquartile range).

Abbreviations: BNP, brain natriuretic peptide; LBBB, left bundle branch block; PVC, premature ventricular contraction; RBBB, right bundle branch block.

*Success vs. failure groups.

[a]Structural heart diseases include valvular heart disease, postoperative state of ventricular septal defect, chronic heart failure with preserved ejection fraction, and dilated cardiomyopathy.

(Figure 4D). small EIA_{10ms}, small $\measuredangle LAT_{Bi\text{-}Uni}$, LAT_{Bi} were defined by cut-off values from receiver-operating characteristic curve analyses.

3.5 | Correlation of indicators

The correlation calculated with Spearman's rank-correlation coefficient revealed mild correlation with EIA_{10ms} and LAT_{Bi} and with EIA_{10ms} and $\measuredangle LAT_{Bi\text{-}Uni}$. However, EIA_{10ms} and $\measuredangle LAT_{Bi\text{-}Uni}$ demonstrated almost no correlation (Figure 5A–C).

4 | DISCUSSION

4.1 | Major findings

This study validated indicators of ablation success for PVCs on high-density mapped cardiac surfaces as prediction models. Main findings are as follows: (1) EIA_{10ms} showed better discrimination ability on receiver-operating characteristic curve analysis than LAT_{Bi}; (2) optimal cutoff values for ablation success of EIA_{10ms}, $\measuredangle LAT_{Bi\text{-}Uni}$, and LAT_{Bi} by receiver-operating characteristic curve analysis were 1.2 cm^2, 9 ms, and 7 ms, respectively; (3) reclassification table, calibration plots, and decision curve analysis demonstrated better predictability of EIA_{10ms} and $\measuredangle LAT_{Bi\text{-}Uni}$; and (4) unipolar morphology of QS or Q pattern did not necessarily guarantee ablation success. To our knowledge, this study is the first to compare the predictability of EIA and the other indicators of ablation success for PVCs.

4.2 | Previous reports

Herczku et al.[3] reported that EIA_{10ms} of ≤2.3 cm^2 on right ventricular outflow tract predicts ablation success on right ventricular outflow tract in 15 patients. Suzuki et al.[4] showed that 5-ms EIA of ≤0.7 cm^2 predicts ablation success for PVC in 29 patients. LAT was recorded with a 3.5-mm irrigation catheter tip (NaviStar, Biosense Webster; Thermocool SF, Biosense Webster) in those studies, leading to limited median mapping points of 40 to 99.[3,4] On the other hand, high-density LAT mapping was performed using multi-electrode catheters in this study. Therefore, optimal cut-off value of EIA_{10ms} for ablation success was 1.2 cm^2 (≤2.3 cm^2), which reflects more accurate LAT maps.

TABLE 2 Procedural and mapping data.

	All patients $n=35$	Success $n=14$	Failure $n=21$	p value*
Procedural data				
Successful PVC alation at the end	32 (91)	14 (100)	18 (86)	.259
Procedure time (min)	150 ± 39	129 ± 37	165 ± 34	.002
Fluoroscopy time (min)	20 ± 11	15 ± 9	28 ± 11	.002
Total complications	2 (6)	1 (7)	1 (5)	1.000
Access				
Endocardial	35 (100)	14 (100)	21 (100)	1.000
Epicardial	2 (6)	0 (0)	2 (10)	.506
Initial mapped cardiac surface				
Right ventricular outflow tract	17 (49)	8 (57)	9 (43)	.407
Left ventricular outflow tract/ Mitral valve annulus/ posteroseptum	8 (23)	4 (29)	4 (19)	.685
Coronary cusps	10 (29)	2 (14)	8 (38)	.252
Mapping data				
Mapping points of initial mapped cardiac surface	262 (101–1024)	374 (99–1031)	222 (92–985)	.556
EIA_{10ms} (cm^2)	2.1 (0.6–4.1)	0.5 (0.1–1.9)	3.7 (2.0–5.3)	.0002
$\measuredangle LAT_{Bi\text{-}Uni}$ (ms)	13 (8–25)	8 (5–14)	20 (12–27)	.0030
LAT_{Bi} (ms)	13 (8–25)	15 (10–35)	12 (0–20)	.142
Fill threshold	7 (5–9)	8 (5–9)	7 (6–13)	.848

Note: Values are presented as *n* (%), mean ± standard deviation, or median (interquartile range).

Abbreviations: $\measuredangle LAT_{Bi\text{-}Uni}$, local activation time (LAT) differences on unipolar and bipolar electrograms; EIA_{10ms}, 10-ms earliest isochronal map area; IDI, integrated discrimination improvement; LAT_{Bi}, LAT prematurity on bipolar electrograms; PVC, premature ventricular contraction.

*Success vs. failure groups.

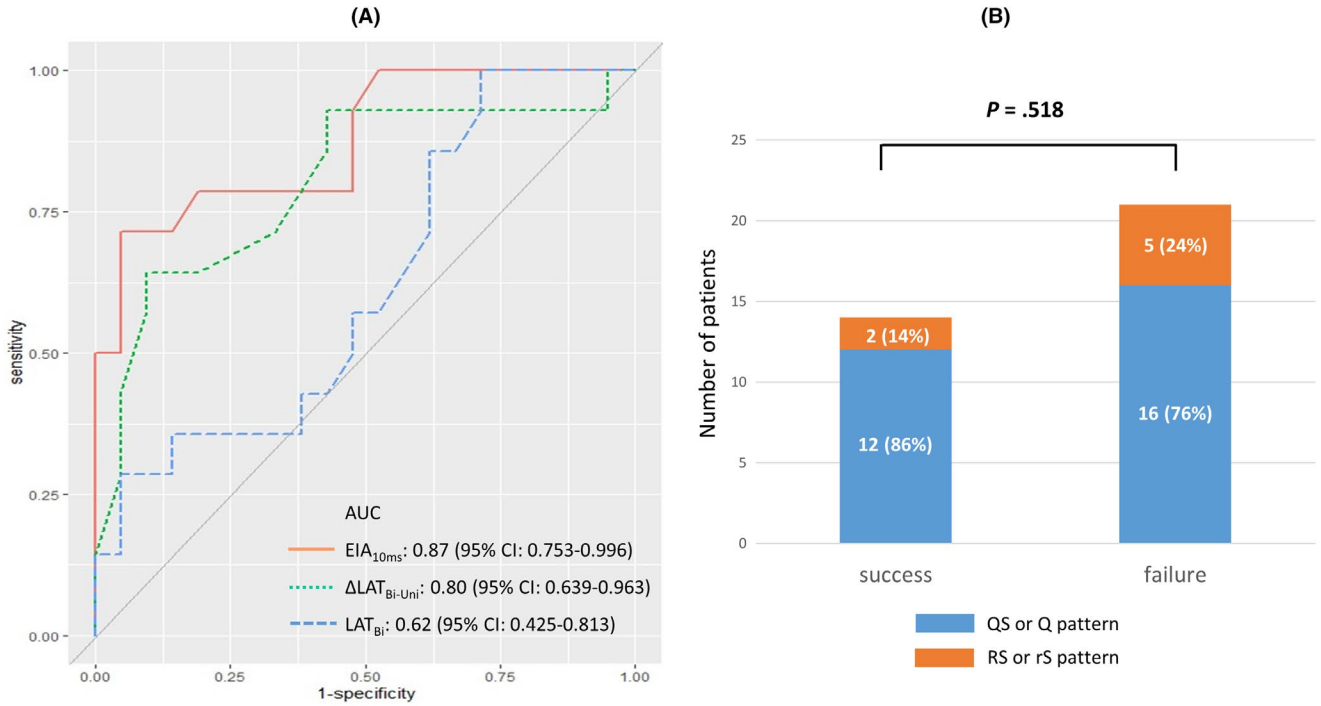

FIGURE 2 Receiver-operating characteristic curve of indicators of ablation success (A) and unipolar morphology between success and failure groups (B). AUC, area under the curve; CI, confidence interval.

TABLE 3 Discrimination ability and reclassification table of indicators of ablation success.

Comparison of AUC			***p* value**
EIA_{10ms} vs. LAT_{Bi}			.014
$\measuredangle LAT_{Bi\text{-}Uni}$ vs. LAT_{Bi}			.278
EIA_{10ms} vs. $\measuredangle LAT_{Bi\text{-}Uni}$			.464
Cutoff value of ablation success	Sensitivity (%)		Specificity (%)
$EIA_{10ms} \leq 1.2\,cm^2$	71.4		95.2
$\measuredangle LAT_{Bi\text{-}Uni} \leq 9$ ms	64.3		90.5
$LAT_{Bi} \geq 7$ ms	100.0		33.4
Reclassification table			
(1) EIA_{10ms} vs. LAT_{Bi}			
Outcome: absent	EIA_{10ms}		
LAT_{Bi}	[0, 0.5)	[0.5,1]	% reclassified
[0,0.5)	14	4	22
[0.5,1]	3	0	100
Outcome: present	EIA_{10ms}		
LAT_{Bi}	[0,0.5)	[0.5,1]	% reclassified
[0, 0.5)	3	7	70
[0.5, 1]	0	4	0
Combined data	EIA_{10ms}		
LAT_{Bi}	[0,0.5)	[0.5,1]	% reclassified
[0, 0.5)	17	11	39
[0.5, 1]	3	4	43
NRI (Continuous) (95% CI)	0.762 (0.140–1.384)		*p* Value: .016
IDI (95% CI)	0.294 (0.119–0.469)		*p* Value: .001
(2) $\measuredangle LAT_{Bi\text{-}Uni}$ vs. LAT_{Bi}			
Outcome: absent	$\measuredangle LAT_{Bi\text{-}Uni}$		
LAT_{Bi}	[0,0.5)	[0.5,1]	% reclassified
[0, 0.5)	15	3	17
[0.5, 1]	2	1	67
Outcome: present	$\measuredangle LAT_{Bi\text{-}Uni}$		
LAT_{Bi}	[0,0.5)	[0.5,1]	% reclassified
[0, 0.5)	2	8	80
[0.5, 1]	3	1	75
Combined data	$\measuredangle LAT_{Bi\text{-}Uni}$		
LAT_{Bi}	[0,0.5)	[0.5,1]	% reclassified
[0, 0.5)	17	11	39
[0.5, 1]	5	2	71
NRI (Continuous) (95% CI)	0.714 (0.111–1.318)		*p* Value: .020
IDI (95% CI)	0.163 (−0.035–0.361)		*p* Value: .108
(3) EIA_{10ms} vs. $\measuredangle LAT_{Bi\text{-}Uni}$			
Outcome: absent	EIA_{10ms}		
$\measuredangle LAT_{Bi\text{-}Uni}$	[0,0.5)	[0.5,1]	% reclassified
[0, 0.5)	13	4	24
[0.5, 1]	4	0	100
Outcome: present	EIA_{10ms}		
$\measuredangle LAT_{Bi\text{-}Uni}$	[0,0.5)	[0.5,1]	% reclassified
[0, 0.5)	1	4	80
[0.5, 1]	2	7	22
Combined data	EIA_{10ms}		
$\measuredangle LAT_{Bi\text{-}Uni}$	[0,0.5)	[0.5,1]	% reclassified
[0, 0.5)	14	8	36
[0.5, 1]	6	7	46
NRI (Continuous) (95% CI)	0.810 (0.212–1.407)		*p* Value: .008
IDI (95% CI)	0.131 (−0.076–0.339)		*p* Value: .215

Abbreviations: AUC, area under the curve; CI, confidence interval; $\measuredangle LAT_{Bi\text{-}Uni}$, local activation time (LAT) differences on unipolar and bipolar electrograms; EIA_{10ms}, 10-ms earliest isochronal map area; IDI, integrated discrimination improvement; LAT_{Bi}, LAT prematurity on bipolar electrograms; NRI, net reclassification improvement.

The other reports stressed note in interpretation of unipolar signals for ablation success for PVCs.[5,6] Sabzwari et al.[5] demonstrated that $\measuredangle LAT_{Bi\text{-}Uni} \geq 15$ ms in LAT map on right ventricular outflow tract predicts origin of left ventricular outflow tract with AUC of 0.77. Higuchi et al.[6] described that the first rapid bipolar deflection that corresponds to a similarly early unipolar deflection was important for ablation success. Those reports demonstrated the importance of characteristics of unipolar potential (i.e., prematurity or sharpness) rather than type of unipolar morphology (i.e., QS or Q pattern). However, these indicators have not been compared as prediction models. Therefore, actual usefulness remained unclear.

4.3 | Importance of analysis of indicators as prediction models

Evaluation methods of prediction models include overall performance, discrimination, reclassification, calibration, and clinical usefulness.[19] Receiver-operating characteristic curve analysis is one of the aspects and cannot necessarily reflect clinical utility.[20] Therefore, NRI and IDI have been complimentarily validated for prediction models.[21] However, NRI and IDI also have limitation for evaluation of predictability.[22] Hilden et al.[22] described that poorly calibrated models may appear advantageous, if NRI and IDI are used to measure gain in prediction performance. Hence, calibration plots and decision curve analysis were also evaluated. Calibration means how accurately prediction models correlate with clinical outcome.[19,23] Decision curve analysis is reported as the method to validate clinical usefulness of prediction models using net benefit.[18]

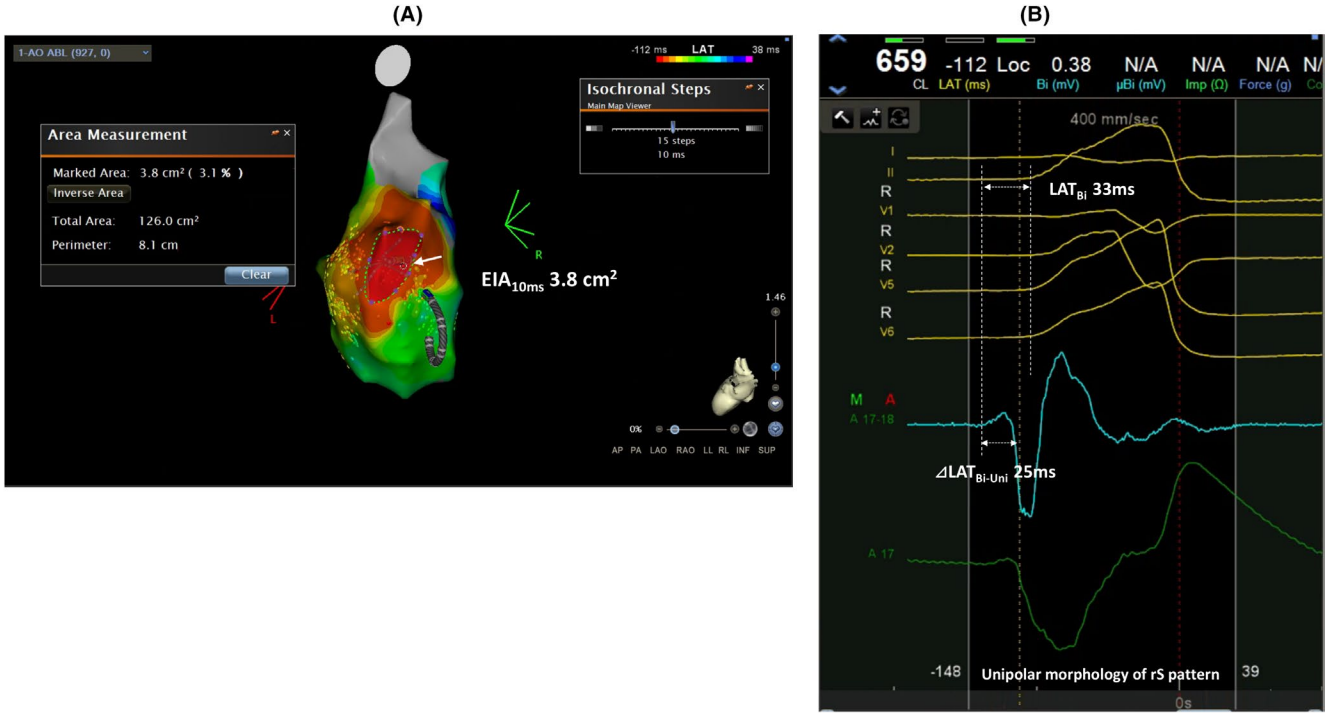

FIGURE 3 (A) An example of unsuccessful ablation on aortic cusps in failure group and the point of earliest steepest dV/dT on unipole (*white arrow*). (B) Intracardiac electrocardiograms at the point of earliest steepest dV/dT on unipole. $\Delta LAT_{Bi\text{-}Uni}$, Local activation time (LAT) differences on unipolar and bipolar electrograms; EIA_{10ms}, 10 ms earliest isochronal map area; LAT_{Bi}, LAT prematurity on bipolar electrograms.

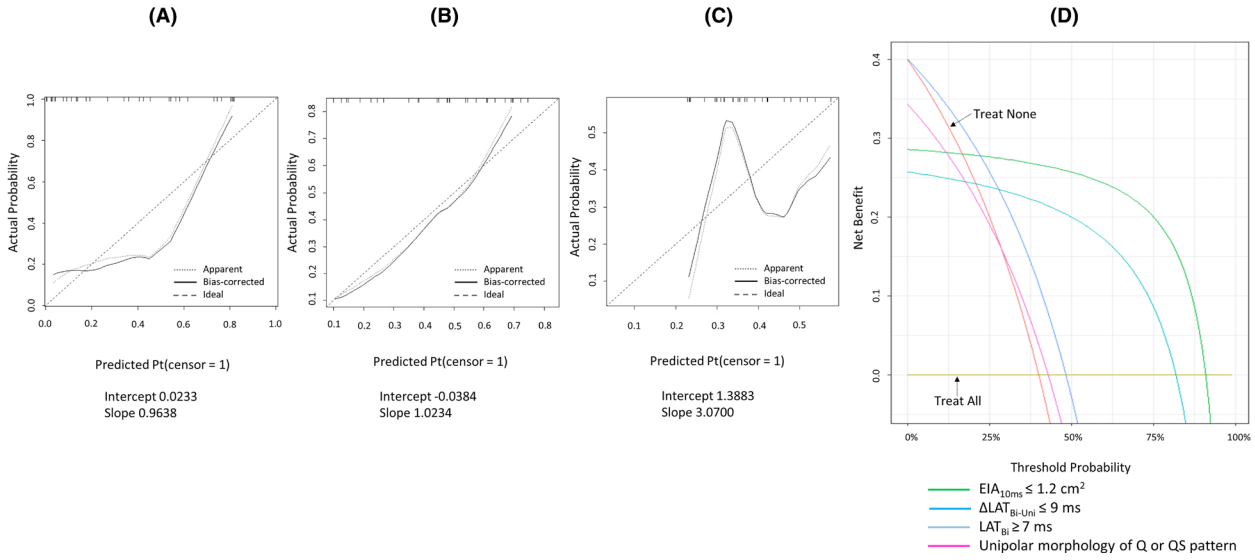

FIGURE 4 Calibration plots of 10 ms earliest isochronal map area (EIA_{10ms}) (A), local activation time (LAT) differences on unipolar and bipolar electrograms ($\Delta LAT_{Bi\text{-}Uni}$) (B), and LAT prematurity on bipolar electrograms (LAT_{Bi}) (C). (D) Decision curve analysis of indicators for ablation success.

4.4 | Clinical implications

Several indicators on 12-lead electrocardiograms for diagnosis of origins of PVCs have been reported.[10–14] However, those indicators can be influenced by anatomical varieties or structural heart diseases. On the other hand, recent innovations in multipolar mapping catheters provide rapid and more accurate LAT maps.[9] The automated algorithm annotating unipolar steepest dV/dT equipped in CARTO3 system also can visualize stable LAT maps. Furthermore, evaluation of EIA_{10ms}, $\Delta LAT_{Bi\text{-}Uni}$, and LAT_{Bi} in high-density LAT maps could enable avoiding unnecessary ablation on mapped cardiac surfaces, leading to safer and shorter procedures.

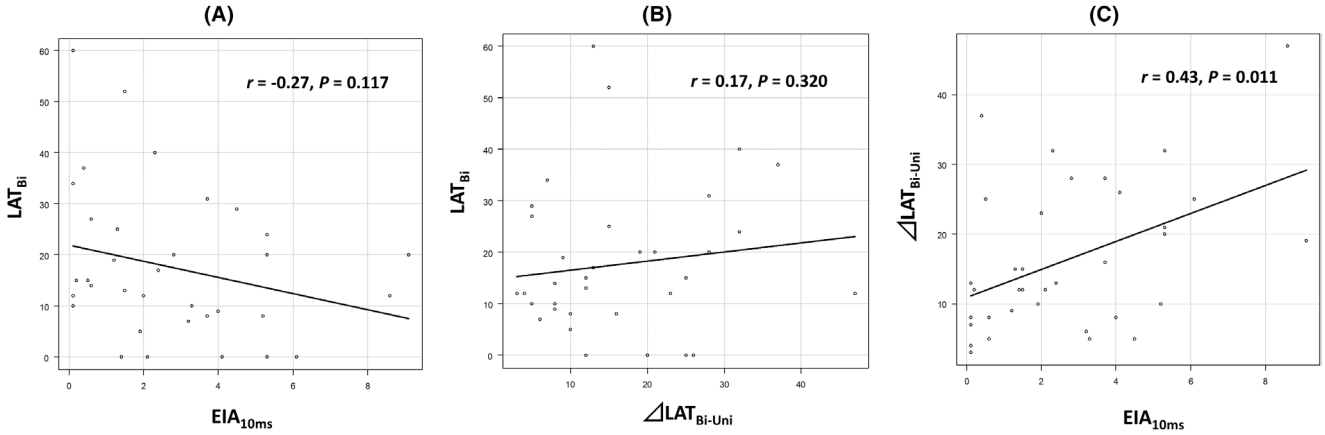

FIGURE 5 Correlation of 10 ms earliest isochronal map area (EIA_{10ms}) and local activation time (LAT) prematurity on bipolar electrograms (LAT_{Bi}) (A), LAT differences on unipolar and bipolar electrograms ($\Delta LAT_{Bi\text{-}Uni}$) and LAT_{Bi} (B), and EIA_{10ms} and $\Delta LAT_{Bi\text{-}Uni}$ (C).

4.5 | Study limitations

First, the number of patients was relatively small, although sample size was estimated. Second, internal and external validation were not necessarily performed for all statistical methods as previously described,[24] leading to possibility of statistical overfitting of evaluated data. Third, prematurity of LAT_{Bi} in mapped cardiac surfaces and the contralateral cardiac surfaces was not simultaneously compared for detecting optimal ablation site as previously reported.[25] Fourth, EIA could be affected by the burden of PVCs. Finally, local variations of cardiac surfaces regarding running of cardiac fibers, diseased areas with structural heart diseases, or epicardial fat can influence on varieties of the indicators. In PVCs originating from left ventricular summit, eccentric activation patterns were reported in some cases,[26] which might affect EIA.

5 | CONCLUSION

EIA_{10ms} and $\Delta LAT_{Bi\text{-}Uni}$ on mapped cardiac surfaces demonstrated better predictability of ablation success for PVC than LAT_{Bi} and unipolar morphology of QS or Q pattern.

ACKNOWLEDGMENTS

We thank Mr. John Martin for proofreading the English of this manuscript.

FUNDING INFORMATION

This research did not receive any specific grant from funding agencies in the public, commercial, or not-for-profit sectors.

CONFLICT OF INTEREST STATEMENT

All the authors declare no conflicts of interest.

DATA AVAILABILITY STATEMENT

The data underlying this article will be shared on reasonable request to the corresponding authors.

ETHICS STATEMENT

The study protocol complied with the Declaration of Helsinki and was approved by the Institutional Review Board of the Higashiyamato Hospital (local ethics committee number: 2023–026).

CONSENT

All patients provided written informed consent.

REFERENCES

1. Cronin EM, Bogun FM, Maury P, Peichl P, Chen M, Namboodiri N, et al. 2019 HRS/EHRA/APHRS/LAHRS expert consensus statement on catheter ablation of ventricular arrhythmias. Heart Rhythm. 2020;17:e2–e154.
2. Lee GK, Klarich KW, Grogan M, Cha YM. Premature ventricular contraction-induced cardiomyopathy: a treatable condition. Circ Arrhythm Electrophysiol. 2012;5:229–36.
3. Herczku C, Berruezo A, Andreu D, Fernández-Armenta J, Mont L, Borràs R, et al. Mapping data predictors of a left ventricular outflow tract origin of idiopathic ventricular tachycardia with V3 transition and septal earliest activation. Circ Arrhythm Electrophysiol. 2012;5:484–91.
4. Suzuki M, Nitta J, Hayashi Y, Lee K, Watanabe K, Hirao T, et al. The efficacy of isochronal 3D mapping-based ablation of ventricular arrhythmia. Int Heart J. 2017;58:495–9.
5. Sabzwari SRA, Rosenberg MA, Mann J, Cerbin L, Barrett C, Garg L, et al. Limitations of unipolar signals in guiding successful outflow tract premature ventricular contraction ablation. JACC Clin Electrophysiol. 2022;8:843–53.
6. Higuchi K, Yavin HD, Sroubek J, Younis A, Zilberman I, Anter E. How to use bipolar and unipolar electrograms for selecting successful ablation sites of ventricular premature contractions. Heart Rhythm. 2022;19:1067–73.
7. De Bakker JMT, Hauer RNW, Simmers TA. Activation mapping: unipolar versus bipolar recording. In: Zipes DP, Jalife J, editors. Cardiac electrophysiology: from cell to bedside. 2nd ed. Philadelphia, PA: W.B. Saunders; 1995. p. 1068.
8. Sorgente A, Epicoco G, Ali H, Foresti S, de Ambroggi G, Balla C, et al. Negative concordance pattern in bipolar and unipolar recordings: an additional mapping criterion to localize the site of origin of focal ventricular arrhythmias. Heart Rhythm. 2016;13:519–26.
9. Sousa PA, Barra S, Cortez-Dias N, Khoueiry Z, Paulo J, António N, et al. Multielectrode mapping for premature ventricular

contraction ablation - a prospective, multicenter study. Int J Cardiol. 2023;383:33–9.
10. Ito S, Tada H, Naito S, Kurosaki K, Ueda M, Hoshizaki H, et al. Development and validation of an ECG algorithm for identifying the optimal ablation site for idiopathic ventricular outflow tract tachycardia. J Cardiovasc Electrophysiol. 2003;14:1280–6.
11. Tada H, Ito S, Naito S, Kurosaki K, Kubota S, Sugiyasu A, et al. Idiopathic ventricular arrhythmia arising from the mitral annulus: a distinct subgroup of idiopathic ventricular arrhythmias. J Am Coll Cardiol. 2005;45:877–86.
12. Ouyang F, Fotuhi P, Ho SY, Hebe J, Volkmer M, Goya M, et al. Repetitive monomorphic ventricular tachycardia originating from the aortic sinus cusp: electrocardiographic characterization for guiding catheter ablation. J Am Coll Cardiol. 2002;39:500–8.
13. Daniels DV, Lu YY, Morton JB, Santucci PA, Akar JG, Green A, et al. Idiopathic epicardial left ventricular tachycardia originating remote from the sinus of Valsalva: electrophysiological characteristics, catheter ablation, and identification from the 12-lead electrocardiogram. Circulation. 2006;113:1659–66.
14. Kawamura M, Hsu JC, Vedantham V, Marcus GM, Hsia HH, Gerstenfeld EP, et al. Clinical and electrocardiographic characteristics of idiopathic ventricular arrhythmias with right bundle branch block and superior axis: comparison of apical crux area and posterior septal left ventricle. Heart Rhythm. 2015;12:1137–44.
15. Acosta J, Soto-Iglesias D, Fernández-Armenta J, Frutos-López M, Jáuregui B, Arana-Rueda E, et al. Clinical validation of automatic local activation time annotation during focal premature ventricular complex ablation procedures. Europace. 2018;20:f171–f178.
16. Okada Y, Kiguchi T, Irisawa T, Yamada T, Yoshiya K, Park C, et al. Development and validation of a clinical score to predict neurological outcomes in patients with out-of-hospital cardiac arrest treated with extracorporeal cardiopulmonary resuscitation. JAMA Netw Open. 2020;3:e2022920.
17. Vickers AJ, Elkin EB. Decision curve analysis: a novel method for evaluating prediction models. Med Decis Mak. 2006;26:565–74.
18. Van Calster B, Wynants L, Verbeek JFM, Verbakel JY, Christodoulou E, Vickers AJ, et al. Reporting and interpreting decision curve analysis: a guide for investigators. Eur Urol. 2018;74:796–804.
19. Steyerberg EW, Vickers AJ, Cook NR, Gerds T, Gonen M, Obuchowski N, et al. Assessing the performance of prediction models: a framework for traditional and novel measures. Epidemiology. 2010;21:128–38.
20. Cook NR. Use and misuse of the receiver operating characteristic curve in risk prediction. Circulation. 2007;115:928–35.
21. Pencina MJ, D'Agostino RB, Pencina KM, Janssens AC, Greenland P. Interpreting incremental value of markers added to risk prediction models. Am J Epidemiol. 2012;176:473–81.
22. Hilden J, Gerds TA. A note on the evaluation of novel biomarkers: do not rely on integrated discrimination improvement and net reclassification index. Stat Med. 2014;33:3405–14.
23. Van Calster B, McLernon DJ, van Smeden M, Wynants L, Steyerberg EW. Topic group 'evaluating diagnostic tests and prediction models' of the STRATOS initiative. Calibration: the Achilles heel of predictive analytics. BMC Med. 2019;17:230.
24. Collins GS, Reitsma JB, Altman DG, Moons KG; TRIPOD Group. Transparent reporting of a multivariable prediction model for individual prognosis or diagnosis (TRIPOD): the TRIPOD statement. The TRIPOD group. Circulation. 2015;131:211–9.
25. Komatsu Y, Nogami A, Shinoda Y, Masuda K, Machino T, Kuroki K, et al. Idiopathic ventricular arrhythmias originating from the vicinity of the communicating vein of cardiac venous systems at the left ventricular summit. Circ Arrhythm Electrophysiol. 2018;11:e005386.
26. Yamada T, Kumar V, Yoshida N, Doppalapudi H. Eccentric activation patterns in the left ventricular outflow tract during idiopathic ventricular arrhythmias originating from the left ventricular summit: a pitfall for predicting the sites of ventricular arrhythmia origins. Circ Arrhythm Electrophysiol. 2019;12:e007419.

How to cite this article: Nagase T, Kikuchi T, Akai S, Himeno M, Ooyama R, Yoshida Y, et al. Predictability of indicators in local activation time mapping of ablation success for premature ventricular contractions. J Arrhythmia. 2024;40:1432–1441. https://doi.org/10.1002/joa3.13148